



HAL
open science

Vibration Characteristics and Persistence of Poloxamer- or Phospholipid-Coated Single Microbubbles under Ultrasound Irradiation

Hiraku Tabata, Daisuke Koyama, Mami Matsukawa, Kenji Yoshida, Marie
Pierre Krafft

► **To cite this version:**

Hiraku Tabata, Daisuke Koyama, Mami Matsukawa, Kenji Yoshida, Marie Pierre Krafft. Vibration Characteristics and Persistence of Poloxamer- or Phospholipid-Coated Single Microbubbles under Ultrasound Irradiation. *Langmuir*, 2019, 35 (35), pp.11322-11329. 10.1021/acs.langmuir.9b02006 . hal-03018455

HAL Id: hal-03018455

<https://hal.science/hal-03018455>

Submitted on 22 Nov 2020

HAL is a multi-disciplinary open access archive for the deposit and dissemination of scientific research documents, whether they are published or not. The documents may come from teaching and research institutions in France or abroad, or from public or private research centers.

L'archive ouverte pluridisciplinaire **HAL**, est destinée au dépôt et à la diffusion de documents scientifiques de niveau recherche, publiés ou non, émanant des établissements d'enseignement et de recherche français ou étrangers, des laboratoires publics ou privés.

This document is confidential and is proprietary to the American Chemical Society and its authors. Do not copy or disclose without written permission. If you have received this item in error, notify the sender and delete all copies.

Vibration characteristics and persistence of poloxamer- or phospholipid-coated single microbubbles under ultrasound irradiation

Journal:	<i>Langmuir</i>
Manuscript ID	Draft
Manuscript Type:	Article
Date Submitted by the Author:	n/a
Complete List of Authors:	Tabata, Hiraku; Doshisha Daigaku Koyama, Daisuke; Doshisha Daigaku Matsukawa, Mami; Doshisha Univ, Faculty of Science and Engineering Yoshida, Kenji; Chiba University, Center for Frontier Medical Engineering Krafft, Marie Pierre; Université de Strasbourg, Institut Charles Sadron (CNRS), Systèmes Organisés Fluorés à Finalités Thérapeutiques (SOFFT)

SCHOLARONE™
Manuscripts

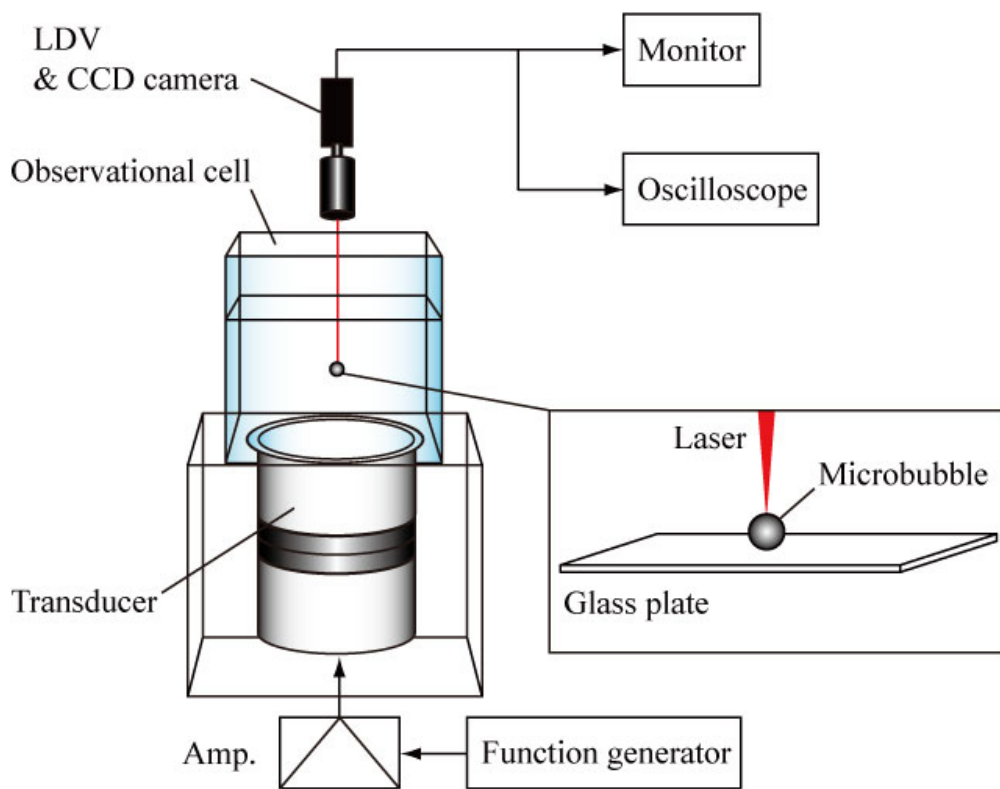
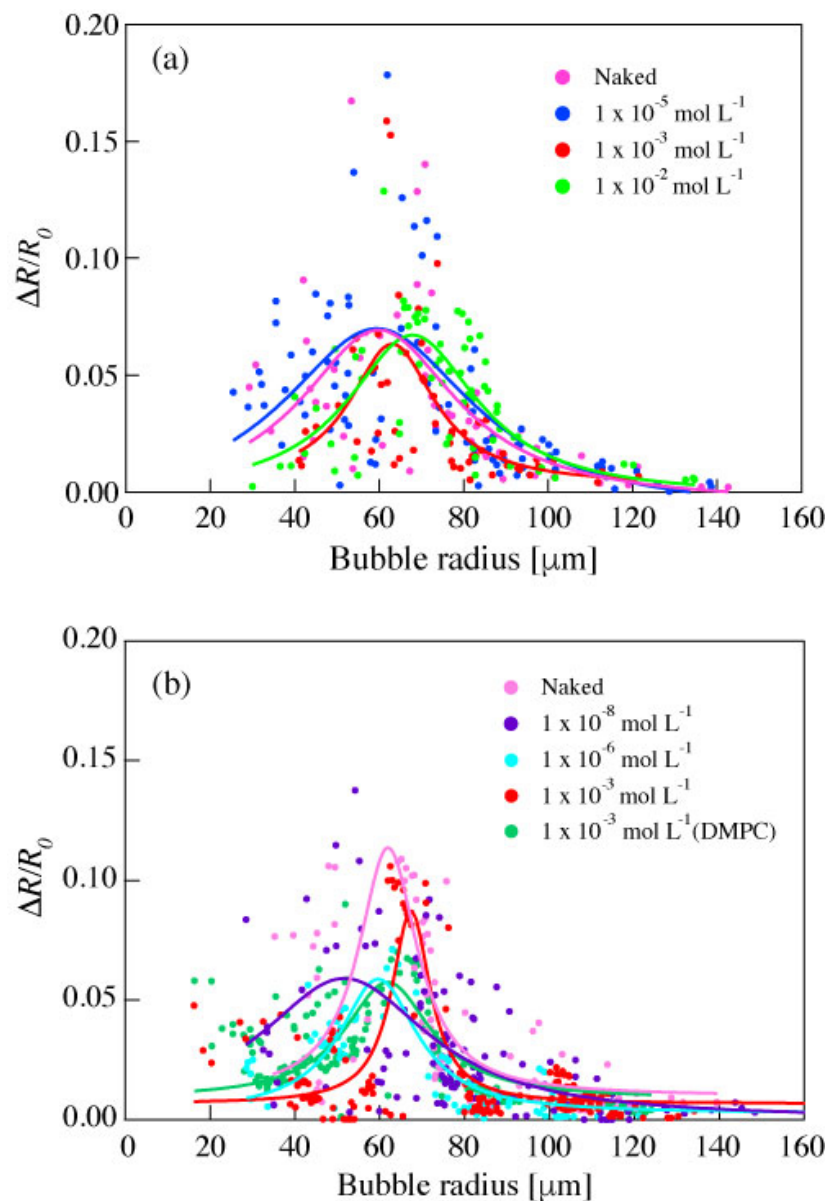


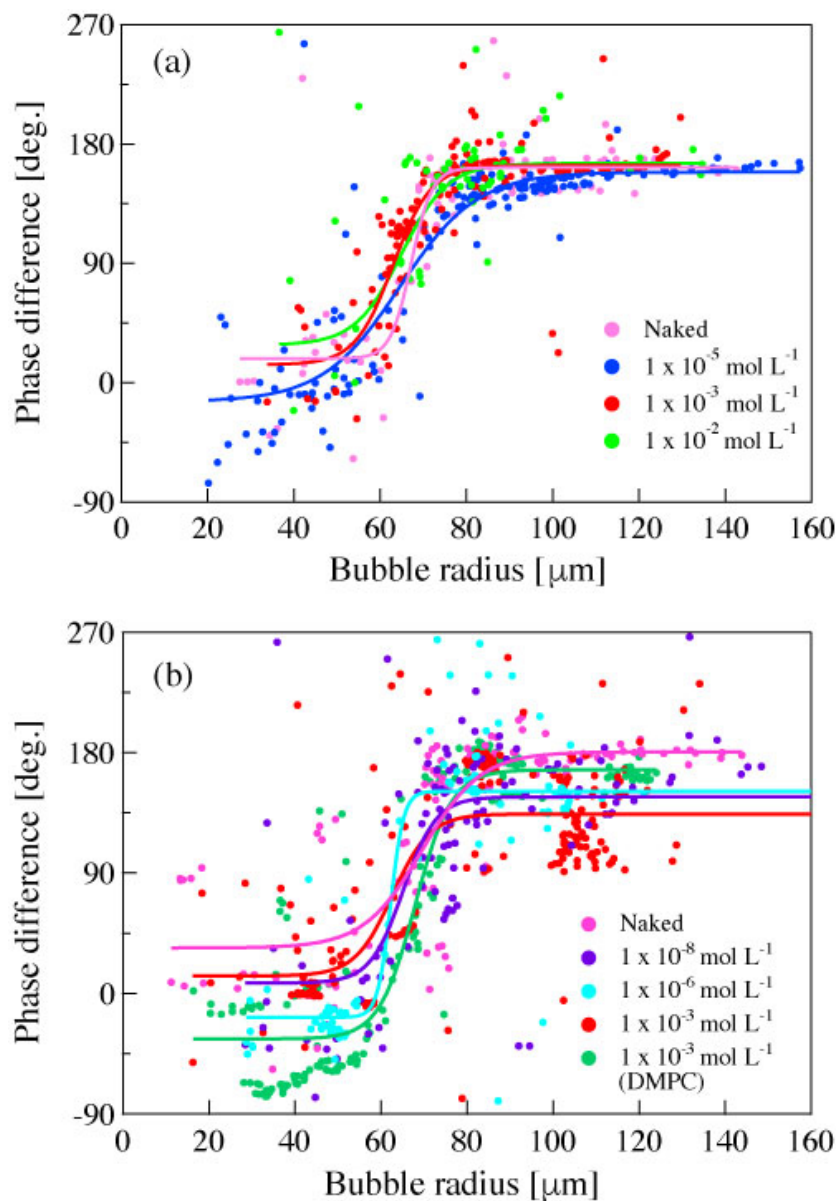
Figure 1. System for single-bubble vibration observation using an ultrasound transducer and laser Doppler vibrometer (LDV).

225x176mm (72 x 72 DPI)



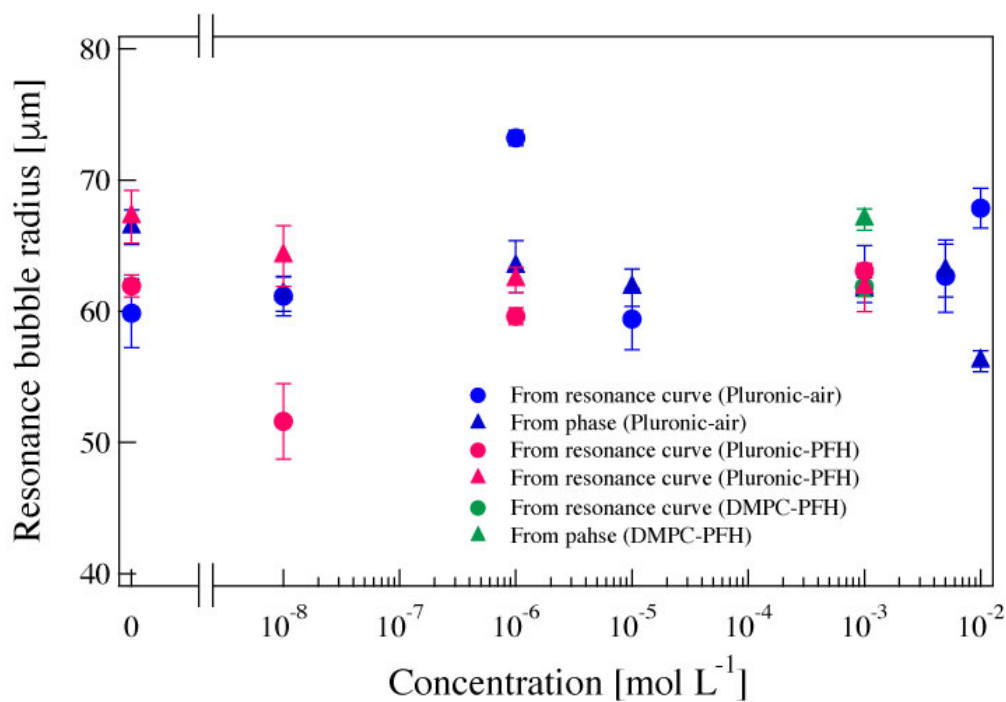
Relationships between the initial bubble radius and normalized displacement amplitude for (a) air-filled microbubbles ($\Delta R/R_0$) coated with Pluronic F-68 at concentrations of 0 (naked), 1×10^{-5} , 1×10^{-3} , and $1 \times 10^{-2} \text{ mol L}^{-1}$ and (b) PFH-filled microbubbles ($\Delta R/R_0$) coated with Pluronic F-68 and DMPC at concentrations of 0 (naked), 1×10^{-8} , 1×10^{-6} , $1 \times 10^{-3} \text{ mol L}^{-1}$ and $1 \times 10^{-3} \text{ mol L}^{-1}$ (DMPC). Fitting curves were obtained using the Lorentz distribution.

176x258mm (72 x 72 DPI)



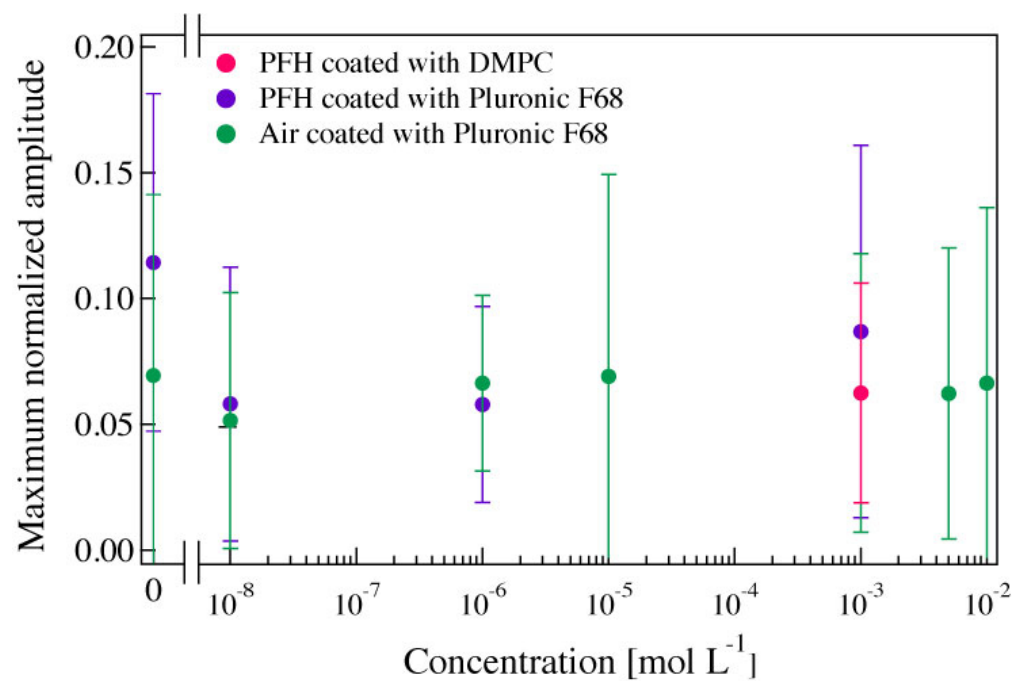
Relationships between bubble radius and phase difference between the sound pressure amplitude and vibration of (a) air-filled microbubbles coated with Pluronic F-68 with concentrations of 0 (naked), 1×10^{-5} , 1×10^{-3} , and $1 \times 10^{-2} \text{ mol L}^{-1}$ and (b) PFH-filled microbubbles ($\Delta R/R_0$) coated with Pluronic F-68 and DMPC at concentrations of 0 (naked), 1×10^{-8} , 1×10^{-6} , $1 \times 10^{-3} \text{ mol L}^{-1}$ and $1 \times 10^{-3} \text{ mol L}^{-1}$ (DMPC). Fitting curves were obtained using the sigmoid distribution.

176x255mm (72 x 72 DPI)



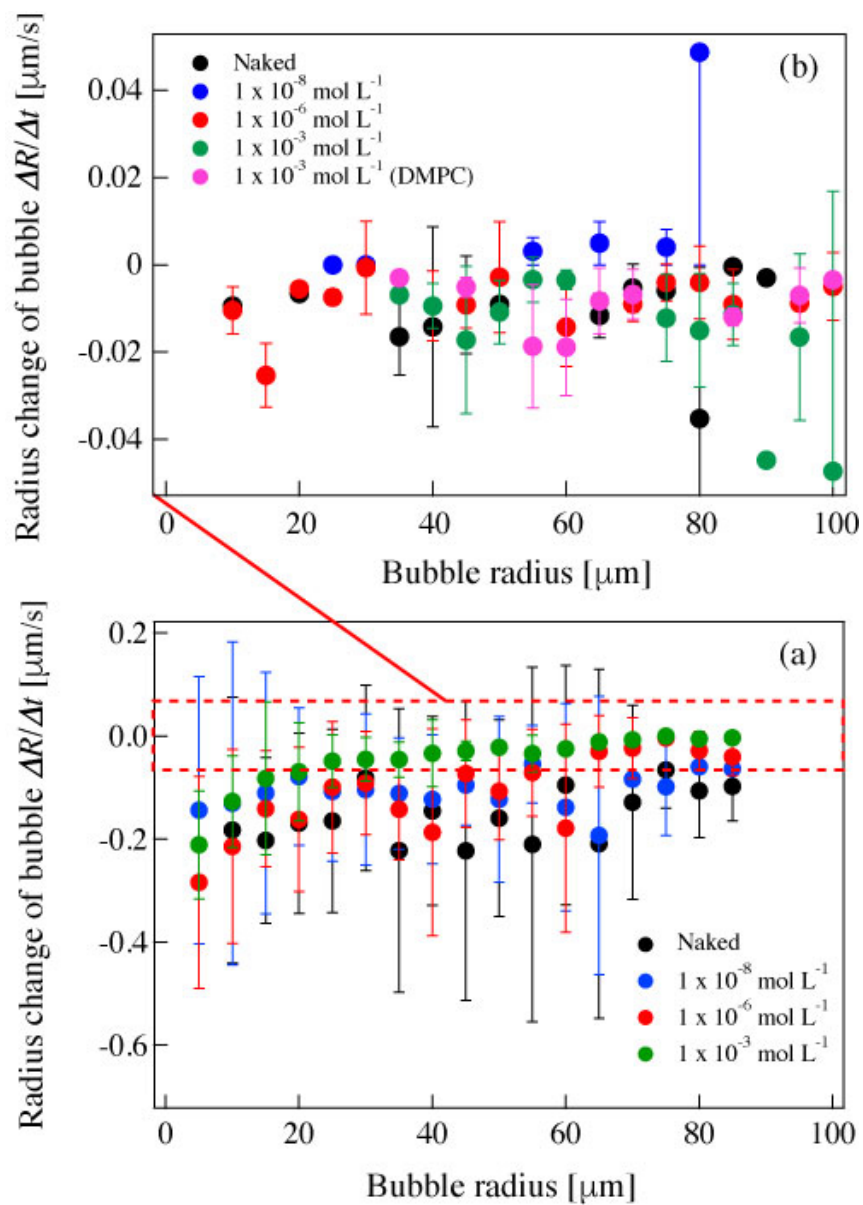
Relationship between Pluronic F-68 concentration and the resonance bubble radius estimated from the resonance curves (Fig. 2) and phase characteristics (Fig. 3). The blue circle and triangle describe air-bubble coated with Pluronic-F68. The pink circle and triangle describe PFH-bubble coated with Pluronic-F68. The green circle and triangle describe PFH-bubble coated with DMPC.

252x176mm (72 x 72 DPI)



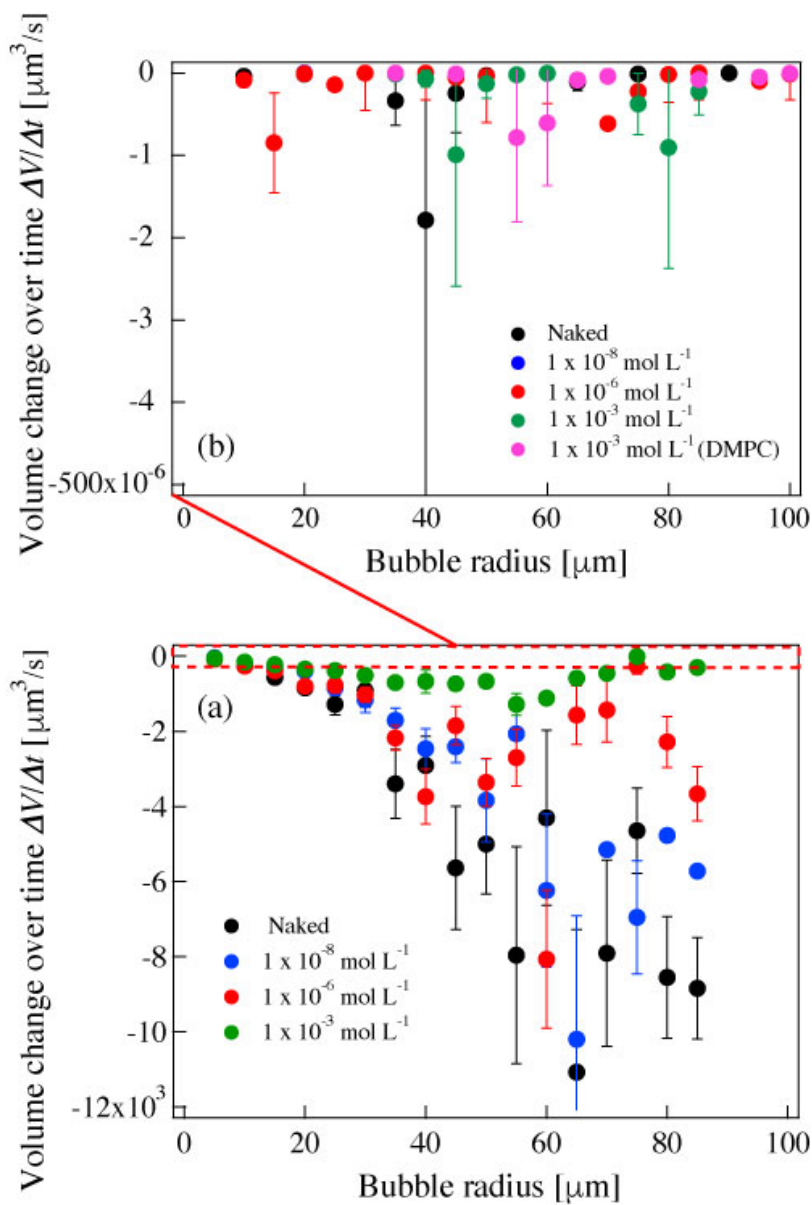
Relationship between Pluronic F-68 concentration and the maximum vibration amplitude of the microbubbles. The green circle describes air-bubble coated with Pluronic-F68. The purple one describes PFH-bubble coated with Pluronic-F68. The pink one describes PFH-bubble coated with DMPC.

260x176mm (72 x 72 DPI)



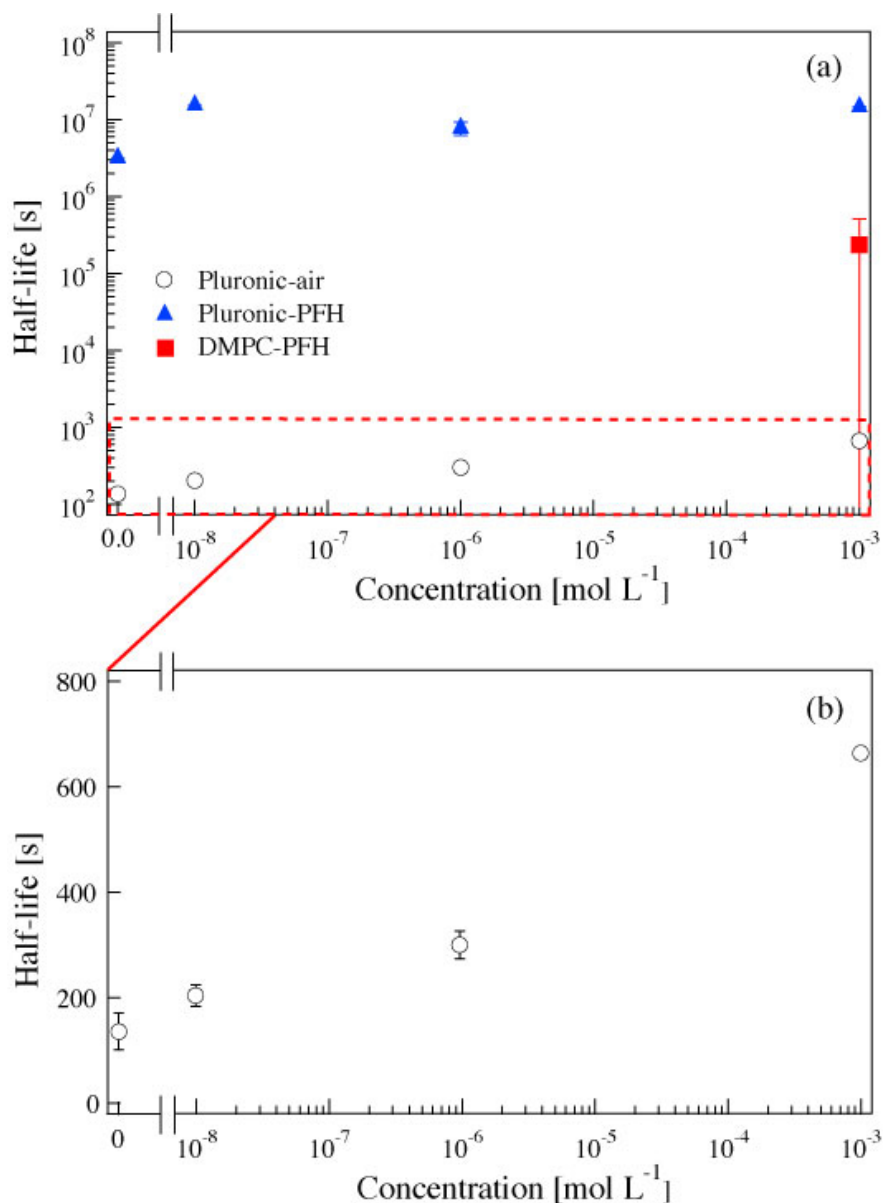
Temporal changes in the radius of (a) air-bubble coated with Pluronic-F68 and (b) PFH-bubble coated with Pluronic-F68 and DMPC.

176x247mm (72 x 72 DPI)



Temporal changes in the volume of (a) air-bubble coated with Pluronic-F68 and (b) PFH-bubble coated with Pluronic-F68 and DMPC.

176x262mm (72 x 72 DPI)



Relationship between concentration of Pluronic F-68 and DMPC and the half-life of microbubbles resonating under ultrasound exposure at 38.8 kHz. The hollow circle shows air-bubble coated with Pluronic-F68 and the triangle shows PFH-bubble coated with Pluronic-F68. The square shows PFH-bubble coated with DMPC.

186x256mm (72 x 72 DPI)

Vibration Characteristics and Persistence of Poloxamer- Phospholipid-Coated Single Microbubbles under Ultrasound Irradiation

Hiraku Tabata¹, Daisuke Koyama^{1,*}, Mami Matsukawa¹, Kenji Yoshida², Marie Pierre Krafft³

¹Faculty of Science and Engineering, Doshisha University, 1-3 Tataramiyakodani, Kyotanabe, Kyoto 610-0321, Japan

²Center for Frontier Medical Engineering, Chiba University, 1-33 Yayoicho, Inage-ku, Chiba 263-8522, Japan

³Institut Charles Sadron (CNRS), University of Strasbourg, 23 rue du Loess, 67034 Strasbourg, France

*dkoyama@mail.doshisha.ac.jp

Abstract: Microbubbles shelled with soft materials are expected to find applications as ultrasound-sensitive drug delivery systems, including through sonoporation. Microbubbles with specific vibrational characteristics and long intravascular persistence are required for clinical uses. To achieve this aim, the kinetics of the microbubble shell components at the gas/liquid interface while being subjected to ultrasound need to be better understood. This paper investigates the vibration characteristics and lifetime of single microbubbles coated with a poloxamer surfactant, Pluronic F-68, and 1,2-dimyristoyl-*sn*-glycero-3-phosphocholine (DMPC) under ultrasound irradiation. Air- and perfluorohexane (PFH)-filled microbubbles coated with Pluronic F-68 and DMPC at several concentrations (0 to 10⁻² mol L⁻¹) were produced. An optical measurement system using a laser Doppler vibrometer and microscope was used to observe the radial vibration mode of single microbubbles. The vibrational displacement amplitude and resonance radius of Pluronic- or DMPC-coated microbubbles were found to depend very little on the concentrations. The resonance radius was around 65 μm at 38.8 kHz under all the experimental conditions investigated. The lifetime of the microbubbles was investigated simultaneously by measuring their temporal change in volume, and it was increased with Pluronic concentration. Remarkably, the oscillation of the bubble has an effect on the bubble lifetime. In other words, the diffusion of the inner gas accelerates at resonance radius.

1. Introduction

Microbubbles are attractive for medical applications such as ultrasound contrast imaging and ultrasound-assisted drug delivery [1-4]. In these applications, the microbubbles are coated with either soft materials such as self-assembled molecular surfactants (e.g. phospholipids) or harder

1
2
3
4
5
6 polymeric materials (e.g. poly(d,l-lactide-co-glycolide) to hinder the diffusion of the internal gases
7 when the bubbles are injected in the vasculature and circulate through the body via blood vessels
8 [5-7]. However, much more stable, polymeric shells considerably dampen the capacity for bubbles to
9 resonate. To serve as drug and gene carriers, bubbles need to persist in the circulation system for
10 hours to days [8-15]. The contraction and expansion of microbubbles under the effect of ultrasound
11 irradiation, that is, bubble vibration, is a critical feature for ultrasound contrast imaging to enhance
12 echo contrast. When used for delivery, collapse of the microbubbles can be initiated by ultrasound
13 irradiation, which induces microjets and provokes the release of the drug or gene to cells. The effects
14 of bubble collapse on tissues and their safety have been investigated [16-19]. Yoshikawa's group
15 reported the effects of ultrasound on deoxyribonucleic acid (DNA) and measured the breaking of
16 doubled-strand DNA under sonication at low ultrasound frequency [20,21]. Cavitation of
17 microbubbles induced by high-intensity ultrasound increases local temperature and can enhance
18 therapeutic effects [22-25].

25
26 There have been many reports on the vibration and collapse of microbubbles under ultrasound
27 irradiation [26-31]. The effect of the shell of the microbubbles on their response to ultrasound
28 vibration can be characterized by comparison with a free air bubble with no surrounding shell.
29 Church [32], Sharker et al. [33], and Marmottant et al. [34] have reported a theoretical model that
30 includes the contributions of shell viscosity and elasticity. Several studies have investigated the
31 effects of a shell on microbubble ultrasound response by comparing experimental and theoretical
32 results [31,35]. Although the acoustic characteristics of a cloud of microbubbles can be measured
33 indirectly through classical pulse echo techniques, we used a dedicated optical observation system
34 fitted with a high-speed microscopic camera that enables direct observation of a single microbubble
35 and is capable of investigating the bubble shell motion, including nonspherical vibration mode [36],
36 collapse [37], and bubble–bubble interactions [38]. However, the standard image resolution of these
37 high-speed cameras is only around 0.5 μm , which is comparable to the bubble size, so large
38 vibrational displacement amplitude ΔR of the bubble excited by large sound pressure is required for
39 observation. Therefore, we previously developed a specific optical observational system that uses a
40 laser Doppler vibrometer (LDV) [39], with which vibrations of small amplitudes (<10 nm) of a
41 single microbubble can be measured through the Doppler effect of the reflected light. Because
42 bubble vibration under ultrasound exposure is essentially a nonlinear phenomenon, the observation
43 of the small-amplitude vibrations of a single microbubble in a linear region can increase our
44 understanding of physical phenomena occurring in microbubbles.

45
46 The microscopic structure of the shell of a bubble and its rheology are the essential factors that
47 determine bubble vibrational characteristics. A monolayer film of amphiphilic molecules is usually
48 formed at the gas/liquid interface on the bubble surface [40-44]. Although the vibration amplitude of
49 microbubbles coated with phospholipids or other surfactants under sonication is restrained by the
50
51
52
53
54
55
56
57
58
59
60

1
2
3
4
5
6 viscoelasticity of the shell, the molecular film prevents the diffusion of the internal gas. Kabalnov et
7 al. [45,46] investigated the lifetime of fluorocarbon-stabilized phospholipid-coated microbubbles in
8 the bloodstream theoretically and experimentally. Bubble lifetime was shown to depend on the gas
9 pressure within the bubble, which is controlled by Laplace pressure, blood pressure, and oxygen
10 metabolism, and the rate of the loss of the inner gas was determined from the bubble [47]. The
11 discrepancy observed between theoretical and experimental data was subsequently determined to be
12 due to a co-surfactant effect between fluorocarbon and phospholipids [48,49]. Considering the
13 clinical use of microbubbles as drug carriers, the effect of ultrasound irradiation of a
14 surfactant-coated bubble on its lifetime needed to be clarified.

15
16 Poloxamers are triblock copolymers consisting of a hydrophobic poly(propylene oxide) (PPO)
17 segment flanked by two hydrophilic poly(oxyethylene oxide) (PEO) chains [40,41]. Poloxamers are
18 candidates of choice for microbubble coating because some of them, including poloxamer 188
19 (Pluronic F-68), are routinely used in applications related to bioprocesses (e.g., to protect cell
20 cultures against shear stress in reactors [50]) and pharmaceuticals (to sensitize cancers resistant to
21 chemotherapy and in personal care products [51]). Pluronic F-68 is commonly used in microbubble
22 preparation as a dispersant and foaming agent [47]

23
24 In our previous work, the vibration characteristics of air- and perfluorohexane (PFH)-saturated air
25 microbubbles coated with Pluronic F-68 were evaluated and the relationship between the vibration
26 characteristics of the microbubble and adsorption conditions of Pluronic F-68 molecules was
27 investigated [44]. The variation of the surface pressure at the air/water or the PFH-saturated
28 air/water interface (at 22 ± 1 °C) as a function of Pluronic F-68 concentration was obtained from
29 dynamic adsorption curves measured by bubble profile analysis tensiometry (see the [Supporting
30 Information](#)). The surface pressure increased (i.e., the surface tension diminished) as the Pluronic
31 concentration increased. The relationship between surface pressure and Pluronic concentration
32 indicated that the molecular film formed at the bubble surface underwent two successive phase
33 transitions.

34
35 The present paper investigates microbubbles coated with the same linear (non-reticulated)
36 polymeric surfactant, Pluronic F-68, when subjected to ultrasound waves, focusing on the
37 relationships between Pluronic concentration and microbubble vibration characteristics and lifetime.
38 We therefore used our specific single-bubble microbubble investigation technology to determine
39 whether and to what extent the poloxamer interferes with the vibrational characteristics (amplitude
40 and phase) and half-life of bubbles subjected to ultrasound irradiation.
41
42
43
44
45
46
47
48
49
50
51
52
53
54
55
56
57
58
59
60

2. Experimental Section

Pluronic F-68 was purchased from Sigma-Aldrich [(PEO)_A(PPO)_B(PEO)_A; CAS Registry No. 9003-11-6; molecular weight (M_w) of $\sim 8400 \text{ g mol}^{-1}$ according to the supplier and $\sim 9050 \text{ g mol}^{-1}$ according to our light scattering experiments]. The degree of polymerization of each block ($N_A = 2 \times 76$, and $N_B = 29$) was calculated from the nominal value of M_w . The polydispersity index ($M_w/M_n = 1.15$, where M_n is the number-average molecular weight) was obtained from gel permeation chromatography using THF as a solvent. The phospholipid, 1,2-dimyristoyl-sn-glycero-3-phosphocholine (DMPC), was purchased from NOF Corporation [CAS Registry No. 18194-24-6; M_w value of 677.9]. Pluronic F-68 and DMPC were used as the surfactants for microbubble coating. Ultrapure water was purchased from Fujifilm Wako Pure Chemical Corporation (CAS Registry No. 7732-18-5).

The vibration characteristics under ultrasound exposure of air- or PFH-saturated air-filled microbubbles coated with Pluronic F-68 or DMPC were measured optically. Figure 1 shows the system used for single-bubble vibration observation. A transparent cubic observation cell (50×50×50 mm) was filled with an aqueous solution of Pluronic F-68 or DMPC with concentrations of 0 to $10^{-2} \text{ mol L}^{-1}$. Air or PFH microbubbles with a radius ranging from 20 to 150 μm were generated in pure water by decompression in a syringe and then deposited gently on the surface of a glass plate fixed at the center of the cell using a micropipette. After the bubbles were attached to the glass plate, the Pluronic F-68 or DMPC molecules in the solution were progressively adsorbed on the bubble surface (gas/water interface). A previous paper by our group [44] reported that the adsorptions of Pluronic F-68 and PFH reaches a plateau after 10 to 60 min. Therefore, Pluronic F-68 or DMPC were allowed to adsorb on the microbubble surface for 60 min before they were exposed to the ultrasound irradiation. A bolt-clamped Langevin-type ultrasound piezoelectric transducer (Fuji Ceramics, Fujinomiya, Japan) was attached to the bottom of the observation cell. By exciting the transducer with a continuous sinusoidal electric signal at a resonance frequency of 38.8 kHz, a half-wavelength longitudinal resonance vibration mode was generated on the transducer and the sound wave was radiated toward the aqueous phase through the bottom of the cell. Multiple reflections of the incident sound wave between the surface of the aqueous solution and bottom of the cell produced an acoustic standing wave field in the vertical direction by controlling the solution level to $n\lambda/2$, where n is an integer and λ is the wavelength of the sound wave in water. The resonance conditions and sound pressure distributions in the cell were maintained at constant values during all the measurements by monitoring the electric admittance of the transducer, which was maximized under the resonance conditions. Because the thickness of the glass plate was much smaller than the wavelength of the standing wave, the plate did not disturb the acoustic field. The microbubbles and glass plate were positioned in the antinodal plane of the standing wave to excite the bubble efficiently. An isolated single microbubble was selected to exclude bubble–bubble interaction effects. The sensor head of an

LDV (NLV2500, PI Polytech, Waldbronn, Germany) with an objective lens (M Plan Apo 20× or 100×, Mitutoyo, Kanagawa, Japan) was positioned above the observation cell to measure the radial vibration of the bubble in the standing wave. The laser beam of the LDV was focused perpendicularly to the top of the bubble's surface to measure the radial component of the vibration through the Doppler effect of the reflected light, and the initial bubble size was determined simultaneously using the CCD camera installed in the sensor head with an image resolution of 1.02 $\mu\text{m pixel}^{-1}$. The size of the focal spot of the LDV beam was 1.5 μm , which is relatively small when compared with the size of the bubble (tens of micrometers) used in this experiment. All the experiments were conducted at a temperature of 22 °C. Altogether samples containing 1209 bubbles with different sizes were measured. Flexural vibration was also generated on the glass plate in the acoustic field and overlapped with the signal of the LDV. However, the vibration component of the glass plate was much smaller than that of the microbubble and can thus be considered negligible.

Because microbubble vibration under ultrasonic exposure is essentially a nonlinear phenomenon, the amplitude of the bubble vibration and vibration mode depend on the sound pressure amplitude; the vibrational amplitude increases nonlinearly and a nonspherical vibration mode involving the surface wave around the bubble surface is generated as the driving sound pressure increases. The sound pressure amplitude at the observational point was measured by a needle hydrophone (Type 8103, Brüel & Kjær, Nærum, Denmark). In our experiments, the sound pressure amplitude was approximately 7.2 kPa, which is sufficiently small to allow observation of the linear spherical vibration of a microbubble [52]. The phase difference between the sinusoidal ultrasound wave to which the bubble was subjected and the bubble vibration driven by ultrasound was measured by monitoring the input current to the transducer to investigate the resonance characteristics of bubble vibrations.

3. Results and Discussion

The influence of the Pluronic F-68 and DMPC shells on micrometric bubble vibration under ultrasound exposure was investigated by measuring the vibrational amplitudes of a single bubble using an LDV under several different conditions. Figure 2 shows the relationship between the initial bubble radius R_0 and the vibrational displacement amplitude of the bubble ΔR , which is called the resonance curve, for microbubbles coated with Pluronic F-68 and DMPC at concentrations ranging from 0 to 10^{-2} mol L⁻¹. Around 60 samples were measured for each concentration. The vertical axis is ΔR normalized by R_0 . An obvious peak of $\Delta R/R_0$ was observed for $R_0 = 40$ to 80 μm under all the conditions investigated. Although the experimental results display large variations because the vibration of a microbubble under ultrasound irradiation is essentially a nonlinear phenomenon, the vibrational characteristics can be described by a Lorentzian fitting curve. This allows determination of the resonance bubble size and maximum ΔR when the sound pressure amplitude is relatively

1
2
3
4
5
6 small (~ 10 kPa) and the bubble vibration is assumed to be in a linear region [52].

7
8 In addition, the resonance bubble size can also be estimated from the phase difference between the
9 driving sound pressure and bubble vibration because the phase difference inverts from 0° to 180°
10 at the resonance size [52]; bubbles smaller (or larger) than the resonance size are contracted (or
11 expanded) by the positive pressure from a continuous sinusoidal sound wave. Figure 3 shows the
12 changes in phase difference with respect to R_0 for several Pluronic F-68 and DMPC concentrations.
13 The phase difference shift depended on surfactant concentration. Compared with that of the data
14 collected for the resonance curves (Fig. 2), the variation in the data is much smaller because the
15 precision of the measurements of the phase difference is less affected by changes in the experimental
16 conditions, such as the contact of the bubble with the plate or the temperature of the solution (the
17 phase difference largely depends on bubble size and driving frequency). A sigmoid fit was used to
18 determine the resonance bubble radius, which is defined as the radius obtained for a phase difference
19 of 90° .
20
21
22
23
24

25 Figure 4 shows the relationship between Pluronic F-68 and DMPC concentrations and the
26 resonance bubble radius estimated from the resonance curves (Fig. 2) and phase difference
27 characteristics (Fig. 3). The plots and error bars in Fig. 4 express the resonance radius determined
28 from each fitting curve and its standard deviation, respectively. These experimental results obtained
29 by two distinct methods are in good agreement. The results concur on the same important points;
30 that is, that the resonance bubble radius is always in the range of 60 to 70 μm and essentially
31 independent of Pluronic or DMPC concentration and inner gas (air or PFH). It should be noted that
32 the resonance radius of a microbubble at 38.8 kHz calculated using a theoretical model for the
33 bubble vibration is 85 μm , and the resonance radius of a microbubble attached to a rigid body is
34 slightly smaller than that of a free microbubble without contact [52].
35
36
37
38
39

40 Figure 5 depicts the relationship between Pluronic F-68 or DMPC concentration and maximum
41 vibrational amplitude of a bubble with the resonance radius estimated from Fig. 4. The vertical axis
42 shows the maximum ΔR normalized by the resonance bubble radius, and the plots and error bars
43 respectively express the peak values of the optimized Lorenz curves and standard deviations
44 calculated from the fitting curves and experimental results. The experimental results in Fig. 4 and 5
45 further confirm that the molecular films of Pluronic F-68 and DMPC have little influence on the
46 vibration of the bubble in the standing-wave acoustic field under the measurement conditions. The
47 radial vibration of a microbubble under low-amplitude ultrasound exposure can be approximated to a
48 simple spring-mass-dashpot mechanical vibration model in the linear region. The numerical models
49 based on Rayleigh-Plesset-like equation have been proposed to describe the dynamical response of
50 an external ultrasound, with parameters for shell characteristics. The shell parameter composed of
51 shell thickness, viscosity, stiffness, friction parameter and surface tension, shift the resonance radius
52 derived from free bubble [31]. Although a higher Pluronic F-68 concentration results in lower
53
54
55
56
57
58
59
60

1
2
3
4
5
6 surface tension at the air/water interface, as shown in the [Supporting Information](#), and the elastic
7 constant of the mechanical spring is decreased by the Pluronic F-68 molecules. These elastic
8 constant and surface tension, which determine resonance radius, depend on the frequency of the
9 ultrasound [31]. The frequency in this experiment, in comparison with ultrasound diagnostic
10 equipment used in clinical practice, is remarkably low. Considering the vibrational characteristics
11 simulated by Rooij et al. and Tu et al. [26-27,31], these parameters affect the resonance radius of a
12 microbubble. In addition, the viscosity of the surrounding molecular film has a damping effect on
13 bubble vibration that is proportional to the vibrational velocity [31]. These effects are enhanced on
14 smaller bubbles driven with higher ultrasound frequency; the vibrational amplitude of
15 micrometer-sized commercial ultrasound contrast agents is damped and the resonance radius
16 increase in the megahertz range. However, our data for the resonance radius (Fig. 4) and the
17 maximum ΔR (Fig. 5) show that the viscoelastic film did not change the resonance size and did not
18 damp the bubble vibration significantly. This is because low ultrasound frequency (38.8 kHz) and
19 large microbubbles (tens of micrometers) were used in the experiments due to our observation
20 system with low image resolution ($1.02 \mu\text{m pixel}^{-1}$).

21
22 A surfactant film is known to hinder the diffusion of the internal gas of microbubbles into the
23 surrounding media and increase the lifetime of the bubble. In addition, the solubility of inner gas
24 also has great relevancy to the life time. According to the work by Kabalnov et al. [45,46], the
25 change in volume of a microbubble goes through three distinct stages. In the first stage, the
26 microbubbles expand (and contract) rapidly until the interfacial tension and pressures in the internal
27 gas and surrounding liquid are balanced. In the second stage, the bubbles contract slowly and the
28 pressure inside the bubbles increases. In the final stage, the gas inside the bubble changes to a liquid
29 and the bubble collapses rapidly; the change rate of a microbubble increases with decreasing bubble
30 size. The life time was evaluated by measuring the temporal change in bubble radius under
31 ultrasound exposure. Figure 6 displays the relationship between bubble radius and radius change rate
32 in the acoustic standing wave. ΔR of the bubbles was almost independent of Pluronic or DMPC
33 concentration and inner gases (see Fig. 2 and 5). The radius change rate was calculated from the
34 change in the average bubble radius between 10 s and 1 hour in the continuous acoustic
35 standing-wave field, and the average values for 2.5- μm radius intervals were plotted. In the
36 experimental results shown in Fig. 6, the change rates were separated clearly between air-filled and
37 PFH-filled bubbles; the change rates of the PFH-filled bubble were almost constant in all the initial
38 bubble radius since PFH has low solubility. On the other hand, the radius change rate of air-filled
39 bubble decreased as the initial radius decreases in all cases because the Laplace pressure $\Delta P = 2\sigma/R$
40 (σ : surface tension; R : bubble radius) increases with decreasing bubble size. In addition, in case of
41 air-filled bubble, higher Pluronic concentrations result in smaller radius changes and smaller error
42 bars because the surfactant film hinders the diffusion of the internal gas.

43
44
45
46
47
48
49
50
51
52
53
54
55
56
57
58
59
60

Figure 7 depicts the relationship between initial radius and volume change rate of the microbubbles in the acoustic standing wave. The volume change was calculated from the experimental results in Fig. 6. Although the variation of the radius was smaller for larger bubbles at air bubble, as shown in Fig. 6, the variation of the volume increased with bubble size. It should be noted that the maximum volume change was observed for a bubble radius of around 60 μm at air-filled bubble, which corresponds to the resonance radius of the microbubbles (see Fig. 4). Therefore, these results mean that the lifetime of the microbubbles depends on their vibrational amplitude under ultrasound exposure, and that a larger vibration amplitude accelerates the diffusion of the internal gas into the surrounding media through the molecular film. The half-life of a microbubble was defined as the time during which the volume of bubbles halved and was calculated from the results in Fig. 7. Figure 8 presents the relationship between Pluronic F-68 concentration and half-life of the microbubbles close to the resonance size under ultrasound exposure. The results clearly demonstrate that a higher concentration of Pluronic F-68 prolongs the lifetime of the air-filled microbubbles.

4. Conclusions and Perspectives

The vibrational characteristics and lifetime of individual air- and PFH-filled microbubbles coated with a film of the block copolymer Pluronic F-68 and phospholipid DMPC exposed to ultrasound were investigated. The vibration of single bubbles in an acoustic standing wave was measured by laser Doppler vibrometry as a function of bubble radius. The maximum vibrational amplitude and resonance size of the bubbles showed little dependence on the presence and concentration of Pluronic. In other words, the polymeric surfactant was found to interfere only minimally with the vibrational qualities and resonance of the microbubbles, which remained similar to those of naked bubbles. On the other hand, the lifetime of the bubbles with coated Pluronic F-68 and DMPC under ultrasound exposure depended on inner gas, bubble size, vibrational amplitude, and concentration of shell material. Remarkably, higher Pluronic concentrations led to longer lifetime.

Acknowledgment

This work was partially supported by the Heiwa Nakajima Foundation. We thank Natasha Lundin, PhD, from Edanz Group (www.edanzediting.com/ac) for editing a draft of this manuscript.

References.

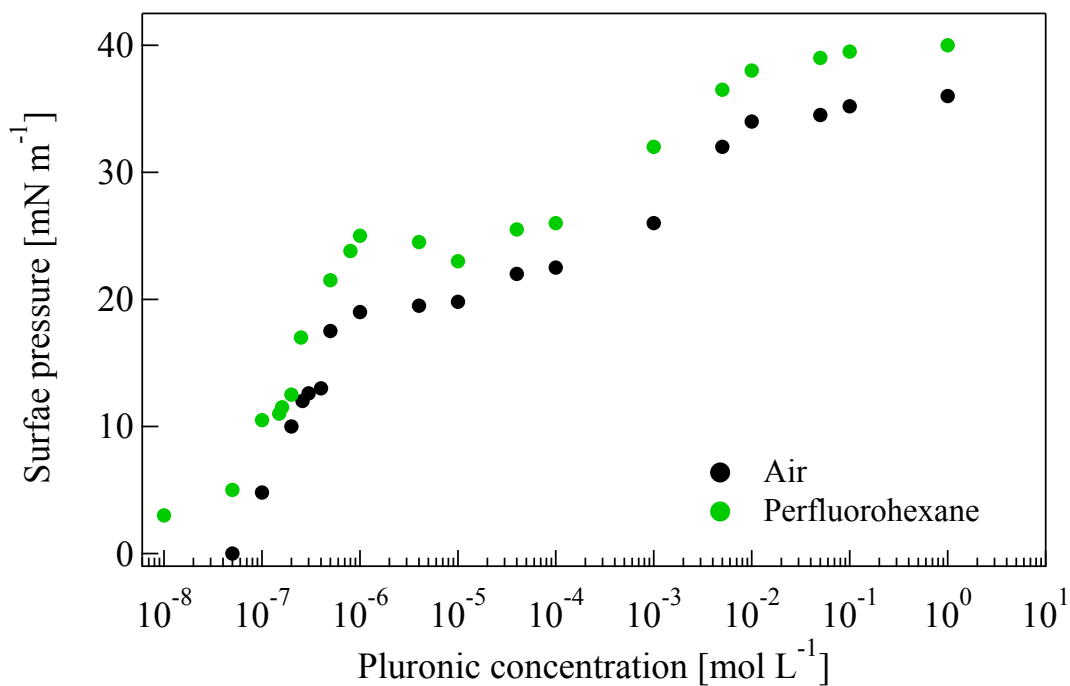
- [1] Zhou, T.; Gai, W.; Yang, H.; Zhang, H.; Hao, M.; Yuan, L.; Liu, J.; Zhang, L. Yang, Y.; Liu, X.; Deng, J.; Zhao, P.; Yang, G.; Duan, Y.; Annexin V conjugated nanobubbles: A novel ultrasound contrast agent for *in vivo* assessment of the apoptotic response in cancer therapy. *J. Control. Release* **2018**, *276*, 113–124.
- [2] Wallace, N.; Wrenn, S. P. Ultrasound triggered drug delivery with liposomal nested

- microbubbles. *Ultrasonics* **2015**, *63*, 31–38.
- [3] Wilson, K. E.; Wang, T. Y.; Willmann, J. K. Acoustic and photoacoustic molecular imaging of cancer. *J. Nucl. Med.* **2013**, *54*, 1851–1854.
- [4] Chong, W. K.; Papadopoulou, V.; Dayton, P. A. Imaging with ultrasound contrast agents: current status and future. *Abdom. Radiol.* **2018**, *43*, 762–772.
- [5] van Rooij, T.; Skachkov, I.; Beekers, I.; Lattwein, K. R.; Voorneveld, J. D.; Kokhuis, T. J. A.; Bera, Deep.; Luan, Y.; van der Steen, A. F. W.; de Jong, N.; Kooiman, K. Viability of endothelial cells after ultrasound-mediated sonoporation: Influence of targeting, oscillation, and displacement of microbubbles. *J. Control. Release* **2016**, *238*, 197–211.
- [6] Lee, M.; Lee, E. Y.; Lee, D.; Park, B. J. Stabilization and fabrication of microbubbles: Applications for medical purposes and functional materials. *Soft Matter* **2015**, *11*, 2067–2079.
- [7] Paefgen, V.; Doleschel, D.; Kiesling, F. Evolution of contrast agents for ultrasound imaging and ultrasound-mediated drug delivery. *Front. Pharmacol.* **2015**, *6*, 197.
- [8] Wang, J.; Barback, C. V.; Ta, C. N.; Weeks, J.; Gude, N.; Mattrey, R. F.; Blair, S. L.; Trogler, W. C.; Lee, H.; Kummel, A. C. Extended lifetime *in vivo* pulse stimulated ultrasound imaging. *IEEE Trans. Med. Imaging* **2018**, *37*, 222–229.
- [9] Jin, Q.; Lin, C. Y.; Kang, S. T.; Chang, Y. C.; Zheng, H.; Yang, C. M.; Yeh, C. K. Superhydrophobic silica nanoparticles as ultrasound contrast agents. *Ultrason. Sonochem.* **2017**, *36*, 262–269.
- [10] Suzuki, R.; Takizawa, T.; Negishi, Y.; Utoguchi, N.; Maruyama, K. Effective gene delivery with novel liposomal bubbles and ultrasonic destruction technology. *Int. J. Pharm.* **2008**, *354*, 49–55.
- [11] Suzuki, R.; Oda, Y.; Utoguchi, N.; Namai, E.; Taira, Y.; Okada, N.; Kadowaki, N.; Kodama, T.; Tachibana, K.; Maruyama, K. A novel strategy utilizing ultrasound for antigen delivery in dendritic cell-based cancer immunotherapy. *J. Control. Release* **2009**, *133*, 198–205.
- [12] Suzuki, R.; Namai, E.; Oda, Y.; Nishiie, N.; Otake, S.; Koshima, R.; Hirata, K.; Taira, Y.; Utoguchi, N.; Negishi, Y.; Nakagawa, S.; Maruyama, K. Cancer gene therapy by IL-12 gene delivery using liposomal bubbles and tumoral ultrasound exposure. *J. Control. Release* **2010**, *142*, 245–250.
- [13] Negishi, Y.; Endo, Y.; Fukuyama, T.; Suzuki, R.; Takizawa, T.; Omata, D.; Maruyama, K.; Aramaki, Y. Delivery of siRNA into the cytoplasm by liposomal bubbles and ultrasound. *J. Control. Release* **2008**, *132*, 124–130.
- [14] Suzuki, R.; Takizawa, T.; Kuwata, Y.; Mutoha, M.; Ishiguro, N.; Utoguchi, N.; Shinohara, A.; Eriguchi, M. Effective anti-tumor activity of oxaliplatin encapsulated in transferrin-PEG-liposome. *Int. J. Pharm.* **2008**, *346*, 143–150.
- [15] Suzuki, R.; Takizawa, T.; Negishi, Y.; Hagiwara, K.; Tanaka, K.; Sawamura, K.; Utoguchi, N.;

- 1
2
3
4
5
6 Nishioka, T.; Maruyama, K. Gene delivery by combination of novel liposomal bubbles with
7 perfluoropropane and ultrasound. *J. Control. Release* **2007**, *117*, 130–136.
- 8
9 [16] Lalzad, A.; Wong, F.; Singh, N.; Coombs, P.; Brockley, C.; Brennan, S.; Ditchfield, M.; Rao,
10 P.; Watloms, A.; Watkins, A.; Saxton, V.; Schneider, M. Knowledge of safety, training, and
11 practice of neonatal cranial ultrasound: A survey of operator. *J. Ultrasound Med.* **2018**, *37*,
12 1411–1421.
- 13
14 [17] McDannold, N.; Vykhodtseva, N.; Hynynen, K. Blood-Brain Barrier disruption induced by
15 focused ultrasound and circulating preformed microbubbles appears to be characterized by the
16 mechanical index. *Ultrasound Med. Biol.* **2008**, *34*, 834–840.
- 17
18 [18] Barnett, S. B.; Maulik, D. Guidelines and recommendations for safe use of doppler ultrasound
19 in perinatal applications. *J. Matern. Fetal Med.* **2001**, *10*, 75–84.
- 20
21 [19] Haar, G. T. Ultrasound bioeffect and safety. *Proc. Inst. Mech. Eng. Part H* **2010**, *224*, 363–
22 373.
- 23
24 [20] Kubota, R.; Yamashita, Y.; Kenmotsu, T.; Yoshikawa, Y.; Yoshida, K.; Watanabe, Y.;
25 Imanaka, T.; Yoshikawa, K. Double-strand breaks in genome-sized DNA caused by ultrasound.
26 *ChemPhysChem* **2017**, *18*, 959–964.
- 27
28 [21] Yoshida, K.; Ogawa, N.; Kagawa, Y.; Tabata, H.; Watanabe, Y.; Kenmotsu, T.; Yoshikawa,
29 Y.; Yoshikawa, K. Effect of low-frequency ultrasound on double-strand breaks in giant DNA
30 molecules. *Appl. Phys. Lett.* **2013**, *103*, 063705.
- 31
32 [22] van Wamel, A.; Kooiman, K.; Hartevelde, M.; Emmer, M.; ten Cate, F. J.; Versluis, M.; de Jong,
33 N. Vibrating microbubbles poking individual cells: Drug transfer into cells via sonoporation. *J.*
34 *Control. Release* **2006**, *112*, 149–155.
- 35
36 [23] Bekeredjian, R.; Grayburn, P. A.; Shohet, R. V. Use of ultrasound contrast agents for gene or
37 drug delivery in cardiovascular medicine. *J. Am. Coll. Cardiol.* **2005**, *45*, 329–335.
- 38
39 [24] Ward, M.; Wu, J.; Chiu, J. F. Ultrasound-induced cell lysis and sonoporation enhanced by
40 contrast agents. *J. Acoust. Soc. Am.* **1999**, *105*, 2951–2957.
- 41
42 [25] Karshafian, R.; Bevan, P. D.; Williams, R.; Samac, S.; Burns, P. N. Sonoporation by
43 ultrasound-activated microbubble contrast agent: Effect of acoustic exposure parameters on
44 cell membrane permeability and cell viability. *Ultrasound Med. Biol.* **2009**, *35*, 847–860.
- 45
46 [26] van Rooij, T.; Luan, Y.; Renaud, G.; van der Steen, A. F. W.; de Jong, N.; Kooiman, K.
47 Acoustical response of DSPC versus DPPC lipid-coated microbubbles. *Proc. 2013 IEEE Int.*
48 *Ultrason. Symp.* **2013**, 310–313.
- 49
50 [27] van Rooij, T.; Luan, Y.; Renaud, G.; van der Steen, A. F. W.; de Jong, N.; Kooiman, K.
51 Non-linear response and viscoelastic properties of lipid-coated microbubbles: DSPC versus
52 DPPC. *Ultrasound Med. Biol.* **2015**, *41*, 1432–1445.
- 53
54 [28] Chatterjee, D.; Sarkar, K. A Newtonian rheological model for the interface of microbubble
55
56
57
58
59
60

- contrast agents. *Ultrasound Med. Biol.* **2003**, *29*, 1749–1757.
- [29] Sijl, J.; Gaud, E.; Frinking, P. J. A.; Arditi, M.; de Jong, N.; Lohse, D.; Versluis, M. Acoustic characterization of single ultrasound contrast agent microbubbles. *J. Acoust. Soc. Am.* **2008**, *124*, 4091–4097.
- [30] van der Meer, S. M.; Dollet, B.; Voormolen, M. M.; Chin, C. T.; Bouakaz, A.; de Jong, N.; Versluis, M.; Lohse, D. Microbubble spectroscopy of ultrasound contrast agents. *J. Acoust. Soc. Am.* **2007**, *121*, 648–656.
- [31] Tu, J.; Guan, J.; Qiu, Y.; Matula, T. J. Estimating the shell parameters of SonoVue® microbubbles using light scattering. *J. Acoust. Soc. Am.* **2009**, *126*, 2954–2962.
- [32] Church, C. C. The effects of an elastic solid surface layer on the radial pulsations of gas bubbles. *J. Acoust. Soc. Am.* **1995**, *97*, 1510–1521.
- [33] Chatterjee, D.; Sarkar, K. A Newtonian rheological model for the interface of microbubble contrast agents. *Ultrasound Med. Biol.* **2003**, *29*, 1749–1757.
- [34] Marmottant, P.; van der Meer, S.; Emmer, M.; Versluis, M.; de Jong, N.; Hilgenfeldt, S.; Lohse, D. A model for large amplitude oscillations of coated bubbles accounting for buckling and rupture. *J. Acoust. Soc. Am.* **2005**, *118*, 3499–3505.
- [35] Yoshida, K.; Morioka, S.; Kagawa, Y.; Koyama, D.; Watanabe, Y. Power-law dependence describing subharmonic generation from a non-spherically oscillating bubble. *Acoust. Sci. & Tech.* **2015**, *36*, 191–200.
- [36] Yoshida, K.; Nakatani, S.; Tsukamoto, A.; Ushida, T.; Watanabe, Y. Effect of collapsing bubble in ultrasonic field on soft material. *Jpn. J. Appl. Phys.* **2008**, *47*, 4200–4204.
- [37] Koyama, D.; Osaki, A.; Kiyan, W.; Watanabe, Y. Acoustic destruction of a micro-capsule having a hard plastic shell. *IEEE Trans. Ultrason., Ferroelect., Freq. Contr.* **2006**, *53*, 1314–1321.
- [38] Yoshida, K.; Fujikawa, T.; Watanabe, Y. Experimental investigation on reversal of secondary Bjerknes force between two bubbles in ultrasonic standing wave. *J. Acoust. Soc. Am.* **2011**, *130*, 135–144.
- [39] Koyama, D.; Kotera, H.; Kitazawa, N.; Yoshida, K.; Nakamura, K.; Watanabe, Y.; Vibration of a single microcapsule with a hard plastic shell in an acoustic standing wave field. *IEEE Trans. Ultrason., Ferroelect., Freq. Contr.* **2011**, *58*, 737–743.
- [40] Muñoz, M. G.; Monroy, F.; Ortega, F.; Rubio, R. G.; Langevin, D. Monolayer of symmetric triblock copolymer at the air-water interface. 1. Equilibrium properties. *Langmuir* **2000**, *16*, 1083–1093.
- [41] Muñoz, M. G.; Monroy, F.; Ortega, F.; Rubio, R. G.; Langevin, D.; Dominique, L. Monolayer of symmetric triblock copolymer at the air-water interface. 2. Adsorption kinetics. *Langmuir* **2000**, *16*, 1094–1101.

- 1
2
3
4
5
6 [42] Svitova, T. F.; Radke, C. J. AOT and Pluronic F68 coadsorption at fluid/fluid interfaces: A
7 continuous-flow tensiometry study. *Ind. Eng. Chem. Res.* **2005**, *44*, 1129–1138.
8
9 [43] Nguyen, P. N.; Waton, G.; Vandamme, T.; Krafft, M. P. Behavior of an adsorbed phospholipid
10 monolayer submitted to prolonged periodical surface density variations. *Angew. Chem., Int.*
11 *Ed.* **2013**, *125*, 6532–6536.
12
13 [44] Ando, Y.; Tabata, H.; Sanchez, M.; Cagna, A.; Koyama, D.; Krafft, M. P. Microbubbles with a
14 self-assembled poloxamer shell and a fluorocarbon inner gas. *Langmuir* **2016**, *32*, 12461 –
15 12467.
16
17 [45] Kabalnov, A.; Klein, D.; Pelura, T.; Schutt, E.; Weers, J. Dissolution of multicomponent
18 microbubbles in the blood stream 1. Theory. *Ultrasound Med. Biol.* **1998**, *24*, 739–749.
19
20 [46] Kabalnov, A.; Bradley, J.; Flaim, S.; Klein, D.; Pelura, T.; Peters, B.; Otto, S.; Reynolds, J.;
21 Schutt, E.; Weers, J. Dissolution of multicomponent microbubbles in the blood stream 2.
22 Experiment. *Ultrasound Med. Biol.*, **1998**, *24*, 751–760.
23
24 [47] Schutt, E. S.; Klein, D. H.; Mattrey, R. M.; Riess, J. G. Injectable microbubbles as contrast
25 agents for diagnostic ultrasound imaging: The key role of perfluorochemicals. *Angew. Chem.,*
26 *Int. Ed.* **2003**, *42*, 3218–3235.
27
28 [48] Nguyen, P. N.; Trinh Dang, T. T.; Waton, G.; Vandamme, T.; Krafft, M. P. A nonpolar,
29 nonamphiphilic molecule can accelerate adsorption of phospholipids and lower their surface
30 tension at the air/water interface. *ChemPhysChem* **2011**, *12*, 2646–2652.
31
32 [49] Szijjarto, C.; Rossi, S.; Waton, G.; Krafft, M. P. Effects of perfluorocarbon gases on the size
33 and stability characteristics of phospholipid-coated microbubbles - Osmotic effect versus
34 interfacial film stabilization. *Langmuir* **2012**, *28*: 1182–1189.
35
36 [50] Tharmalingam, T.; Ghebeh, H.; Wuerz, T.; Butler, M. Pluronic enhances the robustness and
37 reduces the cell attachment of mammalian cells. *Mol. Biotechnol.* **2008**, *39*, 167–177.
38
39 [51] Alakhova, D. Y.; Kabanov, A. V. Pluronic and MDR reversal: An update. *Mol. Pharmaceutics*
40 **2014**, *11*, 2566–2578.
41
42 [52] Yoshikawa, T.; Kotera, H.; Yoshida, K.; Koyama, D.; Nakamura, K.; Watanabe, Y.
43 Measurement of the resonant characteristics of a single bubble vibration by using a laser
44 Doppler vibrometer. *Jpn. J. Appl. Phys.* **2011**, *50*, 07HE04.
45
46 [53] Hoff, L. *Acoustic Characterization of Contrast Agents for Medical Ultrasound Imaging*;
47 Kluwer: Dordrecht, The Netherlands, 2001.
48
49
50
51
52
53
54
55
56
57
58
59
60



Supporting Information: Variation of the surface pressure at an air/water and PFH/water interface as a function of Pluronic F-68 concentration at 22 ± 1 °C.

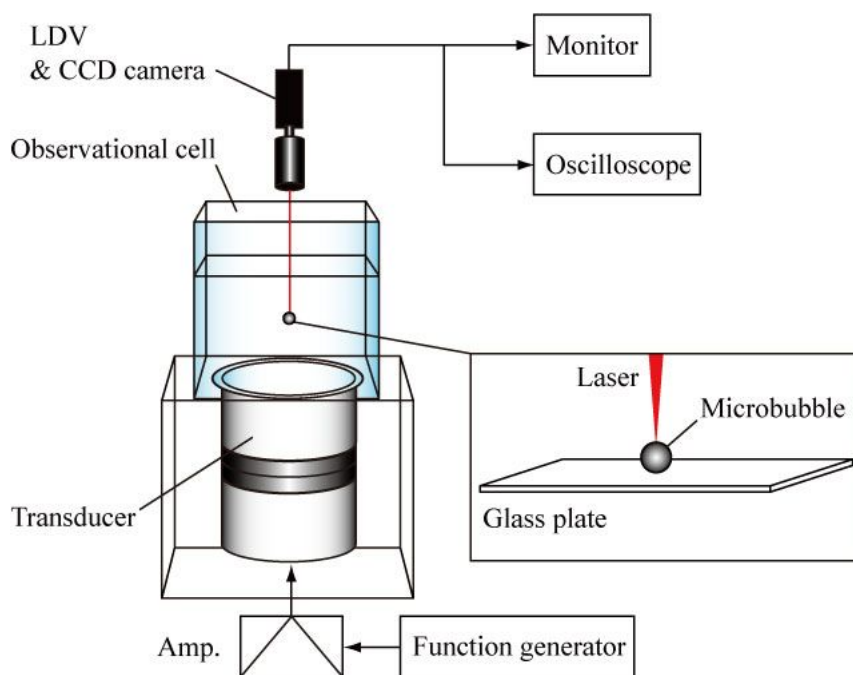


Figure 1. System for single-bubble vibration observation using an ultrasound transducer and laser Doppler vibrometer (LDV).

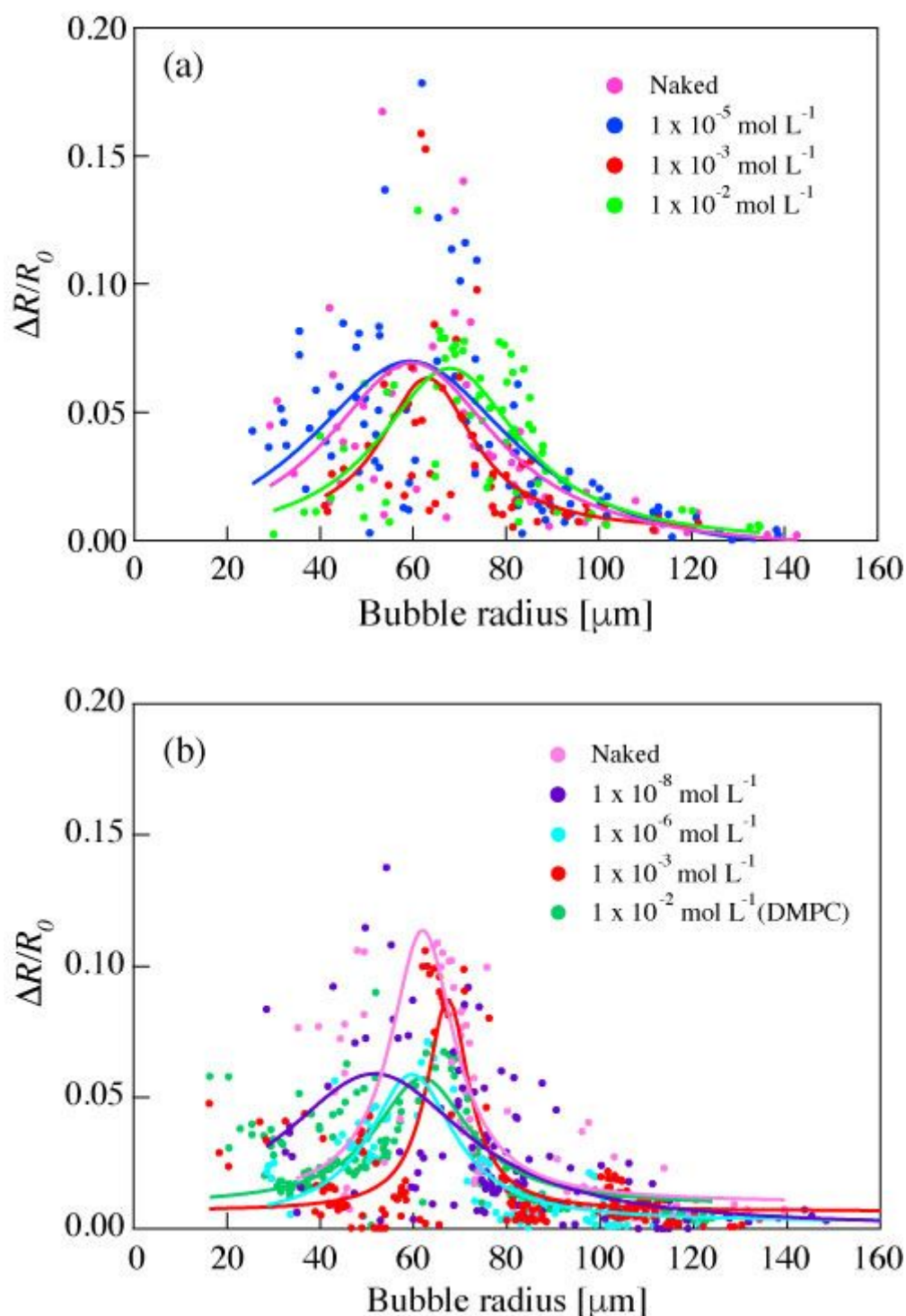


Figure 2. Relationships between the initial bubble radius and normalized displacement amplitude for (a) air-filled microbubbles ($\Delta R/R_0$) coated with Pluronic F-68 at concentrations of 0 (naked), 1×10^{-5} , 1×10^{-3} , and 1×10^{-2} mol L $^{-1}$ and (b) PFH-filled microbubbles ($\Delta R/R_0$) coated with Pluronic F-68 and DMPC at concentrations of 0 (naked), 1×10^{-8} , 1×10^{-6} , 1×10^{-3} mol L $^{-1}$ and 1×10^{-3} mol L $^{-1}$ (DMPC). Fitting curves were obtained using the Lorentz distribution.

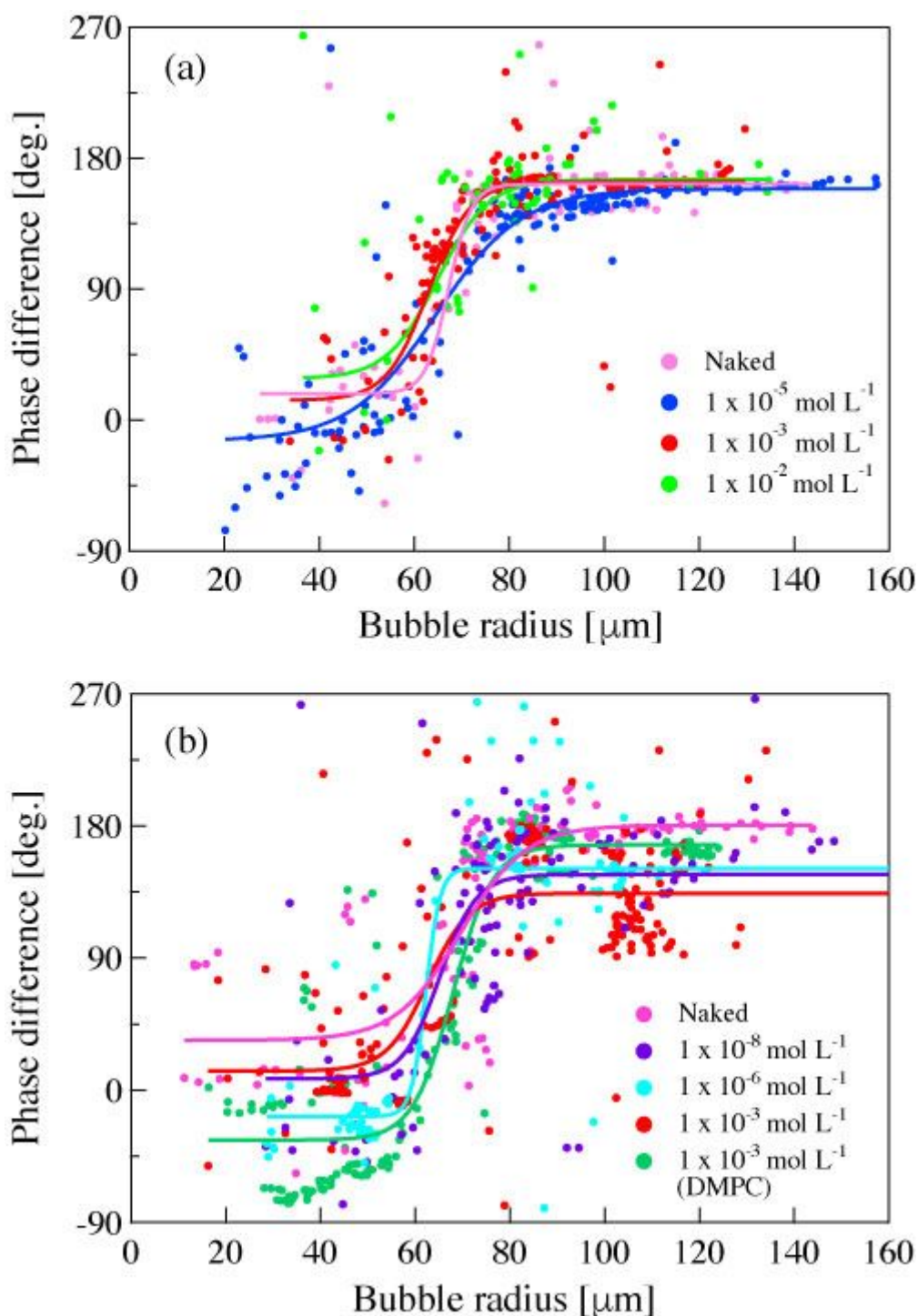


Figure 3. Relationships between bubble radius and phase difference between the sound pressure amplitude and vibration of (a) air-filled microbubbles coated with Pluronic F-68 with concentrations of 0 (naked), 1×10^{-5} , 1×10^{-3} , and 1×10^{-2} mol L $^{-1}$ and (b) PFH-filled microbubbles ($\Delta R/R_0$) coated with Pluronic F-68 and DMPC at concentrations of 0 (naked), 1×10^{-8} , 1×10^{-6} , 1×10^{-3} mol L $^{-1}$ and 1×10^{-3} mol L $^{-1}$ (DMPC). Fitting curves were obtained using the sigmoid distribution.

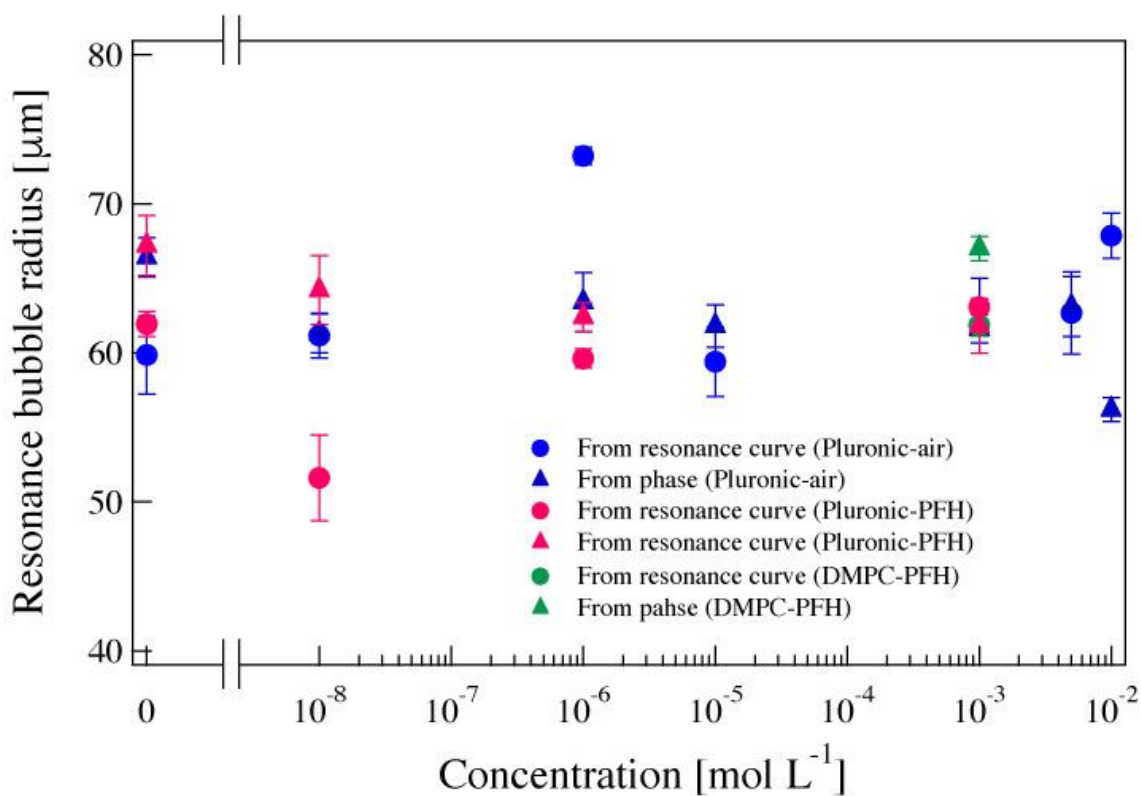


Figure 4. Relationship between Pluronic F-68 concentration and the resonance bubble radius estimated from the resonance curves (Fig. 2) and phase characteristics (Fig. 3). The blue circle and triangle describe air-bubble coated with Pluronic-F68. The pink circle and triangle describe PFH-bubble coated with Pluronic-F68. The green circle and triangle describe PFH-bubble coated with DMPC.

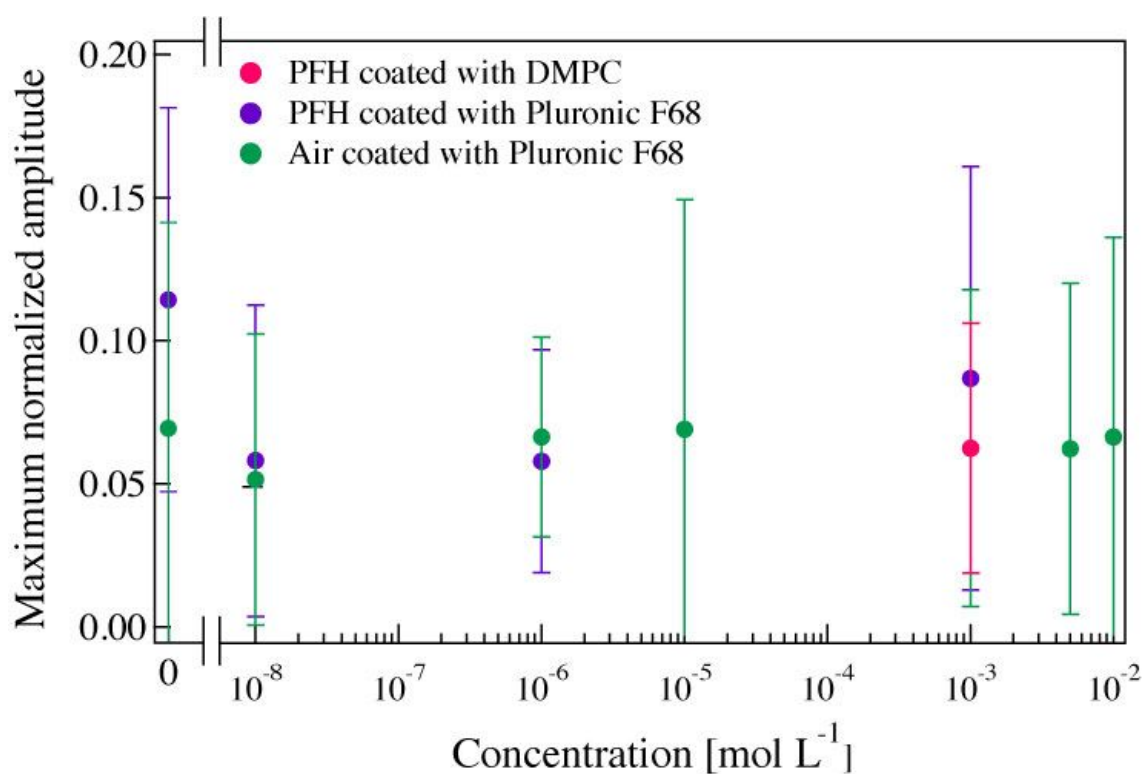


Figure 5. Relationship between Pluronic F-68 concentration and the maximum vibration amplitude of the microbubbles. The green circle describes air-bubble coated with Pluronic-F68. The purple one describes PFH-bubble coated with Pluronic-F68. The pink one describes PFH-bubble coated with DMPC.

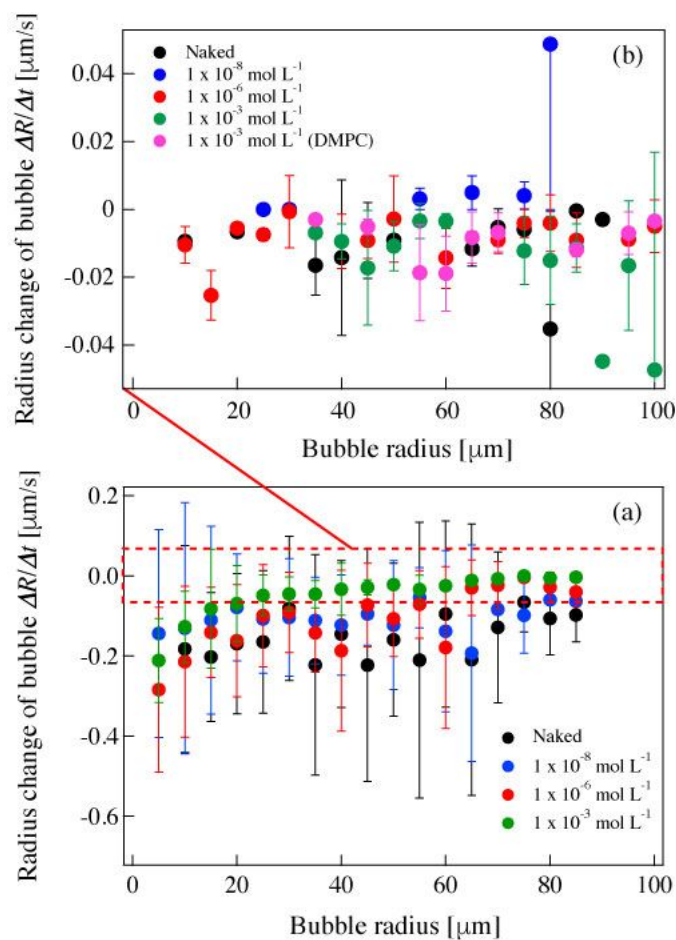


Figure 6. Temporal changes in the radius of (a) air-bubble coated with Pluronic-F68 and (b) PFH-bubble coated with Pluronic-F68 and DMPC.

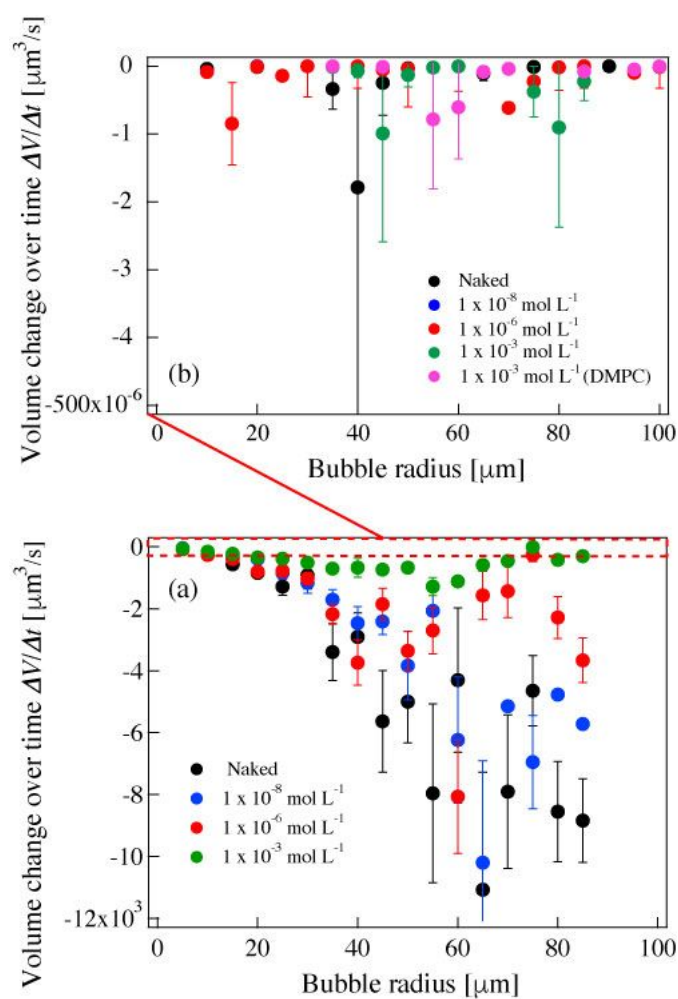


Figure 7. Temporal changes in the volume of (a) air-bubble coated with Pluronic-F68 and (b) PFH-bubble coated with Pluronic-F68 and DMPC.

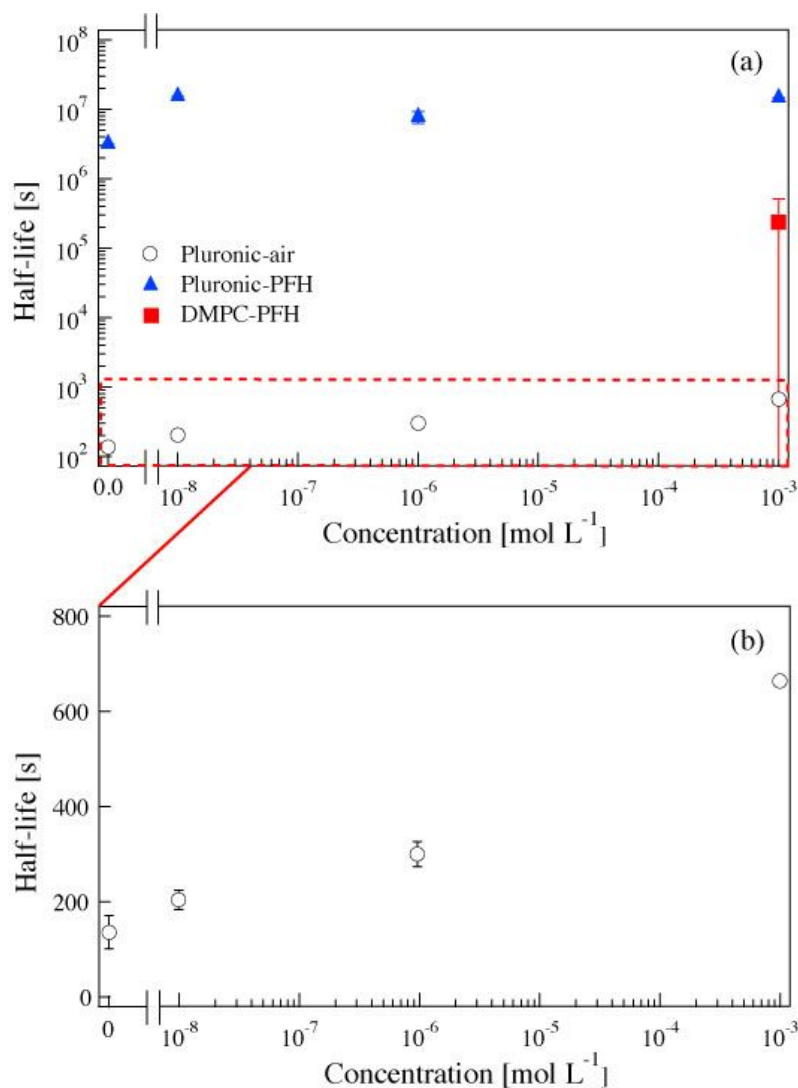


Figure 8. Relationship between concentration of Pluronic F-68 and **DMPC** and the half-life of microbubbles resonating under ultrasound exposure at 38.8 kHz. **The hollow circle shows air-bubble coated with Pluronic-F68 and the triangle shows PFH-bubble coated with Pluronic-F68. The square shows PFH-bubble coated with DMPC.**